PCCP

Structure of $(ZrO_2)_x(SiO_2)_{1-x}$ xerogels ($x = 0.1$, 0.2, 0.3 and 0.4) from FTIR, ^{29}Si and ^{17}O MAS NMR and EXAFS

David M. Pickup,*[a] Gavin Mountjoy,[a] Graham W. Wallidge,[b] Robert J. Newport[a] and Mark E. Smith[b]

[a] *School of Physical Sciences, University of Kent at Canterbury, UK CT2 7NR. E-mail: D.M.Pickup@ukc.ac.uk*

[b] *Department of Physics, University of Warwick, Coventry, UK CV4 7AL*

Received 19th February 1999, Accepted 29th March 1999

A combination of ^{29}Si and ^{17}O MAS NMR, EXAFS and FTIR spectroscopy has been used to study the atomic structure of $(ZrO_2)_x(SiO_2)_{1-x}$ ($x = 0.1$, 0.2, 0.3 and 0.4) xerogels prepared by reacting partially hydrolysed tetraethyl orthosilicate with zirconium(IV) propoxide. Results from $(ZrO_2)_{0.1}(SiO_2)_{0.9}$ samples reveal the oxides to be atomically mixed with no evidence of phase separation. In these samples, the nearest neighbour environment of zirconium is similar to that found in cubic zirconia. In the $(ZrO_2)_{0.4}(SiO_2)_{0.6}$ samples, phase separation occurs with a significant proportion of the zirconium present as amorphous ZrO_2 with a local structure similar to that of monoclinic zirconia. ^{17}O MAS NMR and EXAFS have proven valuable techniques for gauging the level of atomic mixing in these materials.

Introduction

$(ZrO_2)_x(SiO_2)_{1-x}$ materials have attracted interest because of their low expansion coefficients, as well as their good mechanical and chemical resistance.[1] Such materials also exhibit catalytic activity[2] and can be used as supports for other catalysts. Unfortunately, melt-quenched glasses containing significant amounts of ZrO_2 are difficult and expensive to prepare due to the high melting point of zirconia. The sol–gel route from alkoxide precursors offers a low temperature method for preparing mixed oxide glasses.[3]

Many of the properties of $(ZrO_2)_x(SiO_2)_{1-x}$ glasses, such as the degree of atomic mixing, pore size and surface area, depend on the exact preparation conditions. The bulk properties of these materials are related to the connectivity and type of ZrO_x and SiO_x polyhedra present in the structure. Silicon is almost certainly present as SiO_4 tetrahedra whereas zirconium can adopt a range of coordination geometries: *e.g.* 6-fold in catapleiite, $Na_2ZrSi_3O_9 \cdot 2H_2O$, 7-fold in monoclinic ZrO_2 and 8-fold in tetragonal ZrO_2.[4,5] An interesting comparison is to related materials, $(TiO_2)_x(SiO_2)_{1-x}$, where, for $x < 0.2$, titanium adopts tetrahedral coordination within the silica network, whereas for $x \sim 0.4$, small domains of TiO_2 are formed which contain octahedrally coordinated titanium and crystallise into anatase upon heating.[6–8] It is known that zirconium and silicon can form a crystalline oxide zircon, $ZrSiO_4$ (ref. 9) which illustrates that the $(ZrO_2)_x(SiO_2)_{1-x}$ system behaves very differently from its titanium counterpart. The key to understanding the behaviour of the $(ZrO_2)_x(SiO_2)_{1-x}$ materials is to determine how zirconium sits in the silica network and what effect its presence has on the network.

In this work, a combined FTIR, ^{29}Si and ^{17}O MAS NMR, and Zr K-edge EXAFS study on $(ZrO_2)_x(SiO_2)_{1-x}$ ($x = 0$ to 0.4) xerogels has been undertaken to attempt to answer some of the questions raised above. Samples were heat treated to various temperatures up to 750 °C to monitor the effect on the local structure in these glasses.

Experimental

Sample preparation

The samples were prepared using the sol–gel route from the following precursors: tetraethyl orthosilicate, TEOS (Aldrich, 98%), and zirconium(IV) propoxide, $Zr(OPr^n)_4$, 70 wt.% solution in propan-1-ol, Pr^nOH (Aldrich). HCl (Fisons) was used as a catalyst to promote the hydrolysis and condensation reactions and propan-1-ol (Aldrich, 99+%) was used as a mutual solvent.

The method of Yoldas[10] was used to promote homogeneity within the samples. This involved prehydrolysis of the TEOS to maximise the number of Si–OH groups before mixing with the more reactive $Zr(OPr^n)_4$ precursor; the aim being to encourage Si–O–Zr bonding as opposed to Zr–O–Zr bonding which could lead to phase separation. The chosen prehydrolysis conditions were TEOS : Pr^nOH : H_2O in a 1 : 1 : 1 molar ratio in the presence of HCl (pH 1), stirring for 2 h. The appropriate quantity of stock $Zr(OPr^n)_4/Pr^nOH$ solution was diluted further, 1 : 4 by volume with Pr^nOH, before being slowly added to the prehydrolysed TEOS solution while stirring. After one hour, water was added such that the overall water : alkoxide molar ratio was 2. The resulting clear sol was then left to gel: this typically took a few days, depending on composition. It should be noted that all reagents were loaded in a dry box under a N_2 atmosphere and transferred using syringes to avoid absorption of moisture from the atmosphere. Samples for ^{17}O MAS NMR were prepared using 20 mol% ^{17}O enriched water (D-Chem).

All samples were air dried for several days, finely ground and then pumped under vacuum for 24 h to remove any excess solvent. Heat treatments were performed at a heating rate of 5 °C min^{-1} with each temperature maintained for 2 h. Samples were prepared with nominal compositions of $(ZrO_2)_x(SiO_2)_{1-x}$ where $x = 0.1$, 0.2, 0.3 and 0.4. Each sample was heated to 500 and 750 °C. The ^{17}O enriched samples were prepared for the compositions $x = 0.1$ and 0.4 and heat treated at 125, 250, 350, 500 and 750 °C.

FTIR spectroscopy

IR spectra were recorded in diffuse reflectance mode on a Biorad FTS175C spectrometer controlled by Win-IR software. Samples were diluted (1 : 10 by weight) in dry KBr and scanned over the range 4000–400 cm^{-1} with a resolution of 4 cm^{-1}. Each spectrum was the result of summing 64 scans.

MAS NMR

The ^{29}Si NMR spectra were acquired on a Bruker MSL300 spectrometer operating at 59.6 MHz using MAS at typically 4 kHz with a 2.3 μs (~30° tip angle) pulse and a 20 s recycle delay. A 7 mm Bruker double-bearing probe was used. The delay was sufficient to prevent saturation. The spectra were referenced externally to TMS, tetramethylsilane, (0 ppm). Each spectrum was the sum of 500–1000 scans.

The ^{17}O NMR spectra were acquired on a Chemagnetics CMX300 Infinity spectrometer operating at 40.7 MHz with MAS at typically 15 kHz using a Chemagnetics 4 mm double-bearing probe with a 1–2.5 s recycle delay. The delay was sufficient to prevent saturation. A 90°–τ–180° echo sequence was applied with a short τ delay of 71.4 μs to overcome problems of probe ringing thereby allowing the spectra to be phased correctly. The spectra were referenced externally to H_2O (0 ppm). Each spectrum was the result of ~100 000 co-added scans.

EXAFS spectroscopy

Zr K-edge EXAFS data were collected in transmission mode on station 9.2 at the Daresbury Laboratory SRS using a Si[220] crystal monochromator and 50% harmonic rejection. Ionisation chambers, filled with a mixture of Ar/He or Kr/He at appropriate partial pressures to optimise detector sensitivities, were placed in the beam path before and after the sample. Finely ground samples were diluted in boron nitride and pressed into pellets to give a satisfactory edge jump and absorption. Typically each EXAFS spectrum was the sum of three 45 min scans.

Results and data analysis

FTIR spectroscopy

Figs. 1(a) and (b) show the IR spectra of the $(ZrO_2)_x(SiO_2)_{1-x}$ sol gels unheated and after heating to 750 °C, respectively. The peaks in these spectra have been assigned according to the literature.[11–13] The broad bands at 3550 and 3200 cm^{-1} are due to stretching vibrations involving OH groups. The band at 1640 cm^{-1} is assigned to the H–O–H bending vibration of water. The peaks at 1160, 1070 and 795 cm^{-1} are characteristic of a silica network: the bands at 1160 cm^{-1} and 1070 cm^{-1} are ascribed to the LO and TO components of the asymmetric stretch of the SiO_4 unit, respectively, and the feature at 795 cm^{-1} is due to the symmetric stretch of the SiO_4 unit. The shoulder at 980 cm^{-1} is made up of contributions from Si–(OH) stretches and a Si–O–Zr vibration. The assignment of the feature at 500–600 cm^{-1} region will be discussed in detail later. The sharp weak bands at *ca.* 2900 and 1450 cm^{-1} are due to C–H stretching and bending vibrations, respectively, from organic material remaining in the samples.

MAS NMR

The ^{29}Si MAS NMR spectra were deconvolved by Gaussian fitting using Win-IR software; three signals could be distinguished at −94, −101 and −108 ppm with varying intensities. Each resonance represents a specific degree of Si–O–Si polymerisation. The −94 ppm signal comes from Si sites in a Q^2 configuration, and the −101 and −108 ppm signals come from Q^3 and Q^4 configurations, respectively (Q^n stands for a SiO_4 unit with n bridging oxygens[14]). The results of the Gaussian fitting are summarised in Table 1. Fig. 2 shows a typical fit.

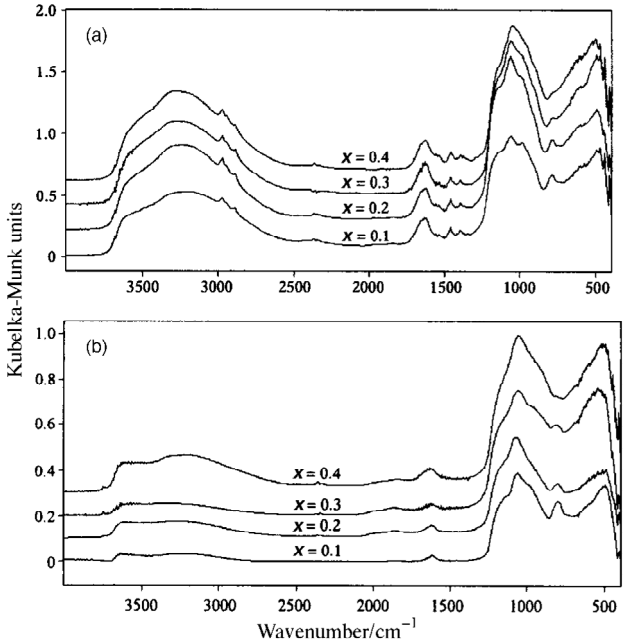

Fig. 1 (a) IR spectra of unheated $(ZrO_2)_x(SiO_2)_{1-x}$ xerogels. (b) IR spectra of $(ZrO_2)_x(SiO_2)_{1-x}$ xerogels after heating to 750 °C for 2 h.

The ^{17}O MAS NMR spectra of the enriched $(ZrO_2)_{0.1}(SiO_2)_{0.9}$ and $(ZrO_2)_{0.4}(SiO_2)_{0.6}$ samples are shown in Figs. 3 and 4, respectively. The spectra are dominated by a resonance which peaks at 0 ppm and shows structure at negative shift due to the quadrupole interaction.[15] This resonance is due to Si–O–Si bridges[16] with a contribution from Si–OH groups.[17] This signal has spinning sidebands from the MAS process at 350 and −350 ppm. The resonances at 295 and 395 ppm observed for the $(ZrO_2)_{0.4}(SiO_2)_{0.6}$ samples are ascribed to Zr–O–Zr bonding and are close to the signals observed from monoclinic zirconia.[18] The signal at around 150 ppm observed for both compositions is due to Zr–O–Si bridges.[18]

EXAFS spectroscopy

The equation for the interpretation of EXAFS data is

$$\chi(k) = \mathrm{AFAC} \sum_j \frac{N_j}{kR_j^2} |f(\pi, k, R_j)| \, e^{-2R_j/\lambda(k)} \times e^{-2\sigma_j^2 k^2} \sin[2kR_j + 2\delta(k) + \psi(k, R_j)]$$

where $\chi(k)$ is the magnitude of the X-ray absorption fine structure as a function of the photoelectron wave vector k. AFAC is the proportion of electrons that perform an EXAFS-type scatter. N_j is the coordination number and R_j is the inter-

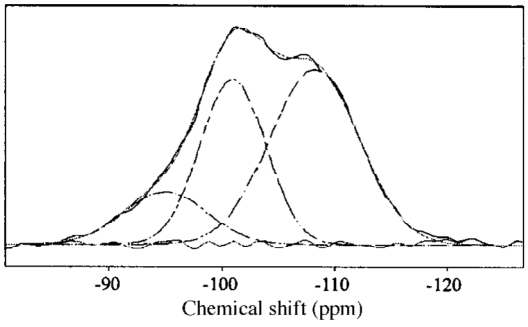

Fig. 2 ^{29}Si MAS NMR spectrum of unheated $(ZrO_2)_{0.1}(SiO_2)_{0.9}$ xerogel showing deconvolution by Gaussian fitting.

Table 1 ^{29}Si NMR data[a]

Sample	Heat treatment /°C	Q^2 FWHM (ppm)	Q^2 δ (ppm)	Q^2 I (%)	Q^3 FWHM (ppm)	Q^3 δ (ppm)	Q^3 I (%)	Q^4 FWHM (ppm)	Q^4 δ (ppm)	Q^4 I (%)
$(ZrO_2)_{0.1}(SiO_2)_{0.9}$	None	8.8(5)	−95.0(5)	14.0	6.8(2)	−100.9(1)	35.1	9.3(1)	−108.2(1)	50.9
	120	10.4(13)	−95.1(15)	12.3	8.1(4)	−101.4(1)	38.4	9.2(2)	−108.5(2)	49.3
	250	9.5(9)	−92.0(11)	4.6	10.6(7)	−100.8(2)	42.7	10.4(2)	−108.3(3)	52.7
	500	11.6(15)	−90.6(15)	4.7	11.2(8)	−100.3(4)	27.2	11.5(2)	−108.6(2)	68.1
	750	10.9(56)	−91.1.(42)	2.4	10.0(13)	−100.0(5)	13.2	12.3(1)	−109.4(1)	84.4
$(ZrO_2)_{0.2}(SiO_2)_{0.8}$	None	11.9(6)	−93.8(6)	22.0	8.0(2)	−100.9(1)	40.2	9.7(2)	−107.8(2)	37.8
	120	14.0(22)	−94.1(26)	19.7	9.7(9)	−101.0(4)	45.6	9.8(5)	−108.1(7)	34.7
	250	12.5(32)	−90.0(40)	9.2	11.8(26)	−100.0(10)	46.1	11.0(6)	−107.7(11)	44.7
	500	11.9(16)	−91.7(21)	8.8	11.4(17)	−101(7)	33.9	11.5(3)	−108.6(6)	57.2
	750	9.0(12)	−94.9(15)	5.5	11.2(28)	−102.3(11)	24.8	12.0(4)	−110.1(7)	69.7
$(ZrO_2)_{0.3}(SiO_2)_{0.7}$	None	11.7(6)	−93.5(6)	33.0	8.3(5)	−100.8(2)	41.7	9.4(5)	−107.8(5)	25.3
	120	11.0(13)	−95.0(15)	33.3	8.0(10)	−101.0(3)	36.6	9.3(8)	−107.6(9)	30.0
	250	12.5(20)	−92.3(28)	17.6	10.7(15)	−100.0(4)	43.9	10.6(5)	−107.8(7)	38.4
	500	10.0(13)	−90.0(15)	9.8	11.2(22)	−99.3(7)	34.1	12.0(6)	−107.8(8)	56.1
	750	12.7(27)	−92.4(39)	9.4	11.7(24)	−100.8(7)	25.1	12.3(4)	−109.2(5)	65.6
$(ZrO_2)_{0.4}(SiO_2)_{0.6}$	None	15.1(5)	−93.0(6)	42.2	11.2(6)	−100.9(3)	42.9	13.9(27)	−106.6(43)	14.9
	120	16.1(9)	−93.5(11)	42.0	10.6(8)	−100.4(6)	37.9	11.7(13)	−106.9(20)	20.1
	250	15.9(10)	−93.2(13)	38.7	11.2(11)	−100.2(5)	35.2	10.6(4)	−107.6(7)	26.1
	500	14.9(33)	−92.9(51)	27.2	11.5(35)	−99.3(12)	23.5	12.5(10)	−107.0(15)	49.3
	750	16.0(31)	−93.0(53)	24.4	12.9(43)	−100.2(18)	26.1	12.8(7)	−107.9(13)	49.5

[a] FWHM, δ and I represent the line width, the ^{29}Si chemical shift and the relative intensity, respectively. Errors: FWHM ±1 ppm, δ ± 1 ppm, I ± 5%.

atomic distance for the jth shell. $\delta(k)$ and $\psi(k, R_j)$ are the phase shifts experienced by the photoelectron, $f(\pi, k, R_j)$ is the amplitude of the photoelectron backscattering and $\lambda(k)$ is the electron mean free path; these are calculated within EXCURV97.[19] The Debye–Waller factor is $A = 2\sigma^2$ in EXCURV97.

The programs EXCALIB, EXBACK and EXCURV97[19] were used to extract the EXAFS signal and analyse the data. Least-squares refinements of the structural parameters of our samples were carried out against the k^3 weighted EXAFS signal to minimise the fit index, FI,

$$\mathrm{FI} = \sum_i [k^3(\chi_i^{\mathrm{T}} - \chi_i^{\mathrm{E}})]^2$$

where χ_i^{T} and χ_i^{E} are the theoretical and experimental EXAFS, respectively. The results of the refinements are reported in

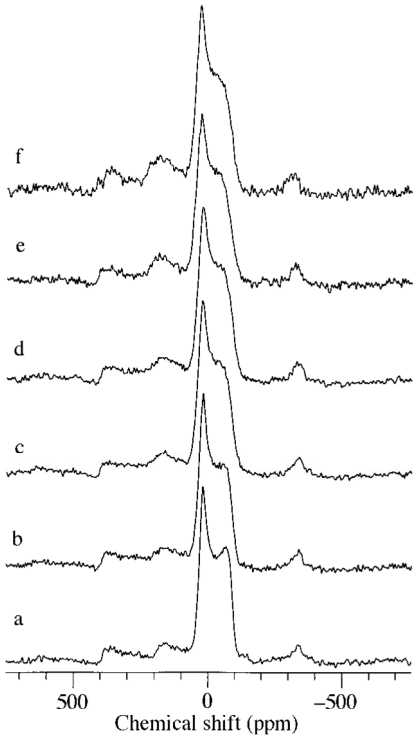

Fig. 3 ^{17}O MAS NMR spectra of a $(ZrO_2)_{0.1}(SiO_2)_{0.9}$ xerogel after various heat treatments: (a) no heat treatment, (b) 125, (c) 250, (d) 350, (e) 500 and (f) 750 °C (peaks at 350 and −350 ppm are spinning sidebands).

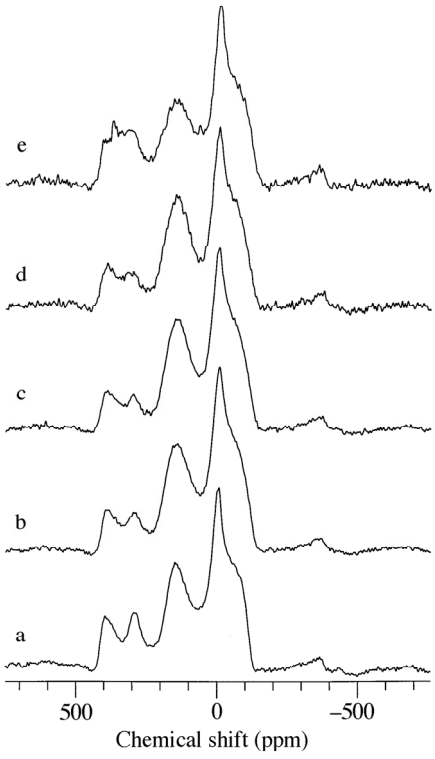

Fig. 4 ^{17}O MAS NMR spectra of a $(ZrO_2)_{0.4}(SiO_2)_{0.6}$ xerogel after various heat treatments: (a) 125, (b) 250, (c) 350, (d) 500 and (e) 750 °C (peaks at 350 and −350 ppm are spinning sidebands).

Table 2 Zr K-edge EXAFS derived structural parameters for reference compounds. The parameters in italics have been fixed

Sample	Shell	N	R/Å	A/Å^2	R_{di} (%)	Crystallographic data[a]/Å
Monoclinic	Zr–O	7	2.13(1)	0.019(2)	36	7O × ~2.054
ZrO_2	Zr–Zr	7	3.46(1)	0.013(1)		7Zr × 3.454
	Zr–Zr	4	3.99(1)	0.018(3)		4Zr × 3.977
	Zr–Zr	1	4.54(3)	0.009(5)		1Zr × 4.540
Tetragonal	Zr–O	4	2.09(1)	0.010(2)	39	4O × 2.065
ZrO_2	Zr–O	4	2.28(3)	0.046(15)		4O × 2.455
	Zr–Zr	12	3.62(1)	0.018(1)		12Zr × 3.67
Cubic	—	—	—	—	—	3O × 2.04
$(Zr, Y)O_{1.87}$	—	—	—	—		4O × 2.23
	—	—	—	—		12Zr × 3.64
Zircon	Zr–O	4	2.12(1)	0.005(2)	38	4O × 2.129
$ZrSiO_4$	Zr–O	4	2.26(1)	0.006(2)		4O × 2.267
	Zr–Si	2	3.00(1)	0.005(2)		2Si × 2.990
	Zr–Zr	4	3.64(1)	0.006(1)		4Zr × 3.625
	Zr–Si	4	—	—		4Si × 3.625

[a] Refs. 5 and 9.

terms of the discrepancy index

$$R_{di} = \frac{\int |[\chi^T(k) - \chi^E(k)]| k^3 \, dk}{\int |\chi^E(k)| k^3 \, dk} \times 100\%$$

Monoclinic and tetragonal zirconia (TOSOH Corporation) were run as reference materials to check the validity of our data analysis and also to allow refinement of the parameter AFAC. The results obtained from our standard materials are summarised in Table 2. The parameters were obtained by fitting the EXAFS data over the range 2.8–20.0 Å^{-1}. In these refinements, the coordination numbers were fixed at values consistent with the crystallographic data available.[5] The errors are the statistical uncertainties calculated by EXCURV97. Also included in Table 2 are the crystallographic data for yttrium stabilised cubic zirconia for comparison. The value obtained for the second Zr–O distance in tetragonal zirconia is shorter than the crystallographic distance; this effect is caused by the addition of Y_2O_3 to our sample to stabilise the tetragonal phase at room temperature.[5] A value of 0.91 for AFAC was derived from the data from the reference compounds; this was used throughout analysis of the data from our sol–gel samples. Zircon, $ZrSiO_4$, (Strem Chemicals) was also run as a standard because this material has similar composition to some of our sol–gel samples. The structural parameters obtained are presented in Table 2. There is good agreement with the crystallographic data, although it should be noted that fitting the EXAFS data with a second silicon shell at ~3.6 Å did not yield the correct Zr–Si distance structural parameters. This is due to the fact that silicon is a weak backscatterer at this distance and therefore this correlation does not have a significant contribution to the EXAFS signal.

The Zr K-edge EXAFS derived parameters of our sol–gel samples are shown in Table 3. The errors are the statistical uncertainties calculated by EXCURV97. Figs. 5 and 6 show the EXAFS data and their Fourier transforms together with

Table 3 Zr K-edge EXAFS derived structural parameters for $(ZrO_2)_x(SiO_2)_{1-x}$ xerogels

Composition	Heat treatment	Shell	N	R/Å	A/Å^2	R_{di} (%)
$(ZrO_2)_{0.4}(SiO_2)_{0.6}$	Room temp.	Zr–O	7.9(5)	2.14(1)	0.023(2)	30
		Zr–Zr	4.2(15)	3.49(1)	0.025(5)	
	500	Zr–O	7.3(4)	2.13(1)	0.026(2)	31
		Zr–Zr	4.2(14)	3.41(1)	0.030(5)	
	750	Zr–O	7.4(5)	2.12(1)	0.028(2)	32
		Zr–Zr	4.3(16)	3.40(1)	0.030(5)	
$(ZrO_2)_{0.3}(SiO_2)_{0.7}$	Room temp.	Zr–O	8.4(6)	2.14(1)	0.029(3)	35
		Zr–Zr	4.9(22)	3.50(1)	0.033(8)	
	500	Zr–O	7.2(6)	2.12(1)	0.029(3)	42
		Zr–Zr	3.6(17)	3.42(1)	0.030(9)	
	750	Zr–O	7.5(6)	2.11(1)	0.033(3)	40
		Zr–Zr	4.3(17)	3.39(1)	0.030(6)	
$(ZrO_2)_{0.2}(SiO_2)_{0.8}$	Room temp.	Zr–O	9.5(9)	2.14(1)	0.038(4)	39
		Zr–Zr	3.4(15)	3.53(3)	0.032(17)	
	500	Zr–O	7.9(8)	2.10(1)	0.033(3)	42
		Zr–Zr	3.5(18)	3.38(2)	0.031(8)	
	750	Zr–O	8.6(8)	2.10(1)	0.040(4)	37
		Zr–Zr	4.4(16)	3.38(1)	0.032(6)	
$(ZrO_2)_{0.1}(SiO_2)_{0.9}$	Room temp.	Zr–O	3.1(4)	2.00(1)	0.006(1)	35
		Zr–O	6.4(13)	2.25(1)	0.031(9)	
		Zr–Zr	0.7(4)	3.37(1)	0.012(6)	
	500	Zr–O	2.3(6)	2.01(1)	0.005(2)	30
		Zr–O	5.2(15)	2.18(3)	0.038(13)	
		Zr–Zr	0.2(2)	3.40(1)	0.006(5)	
	750	Zr–O	2.4(8)	1.98(1)	0.007(2)	31
		Zr–O	4.4(17)	2.15(4)	0.039(17)	
		Zr–Zr	0.5(4)	3.38(2)	0.013(7)	

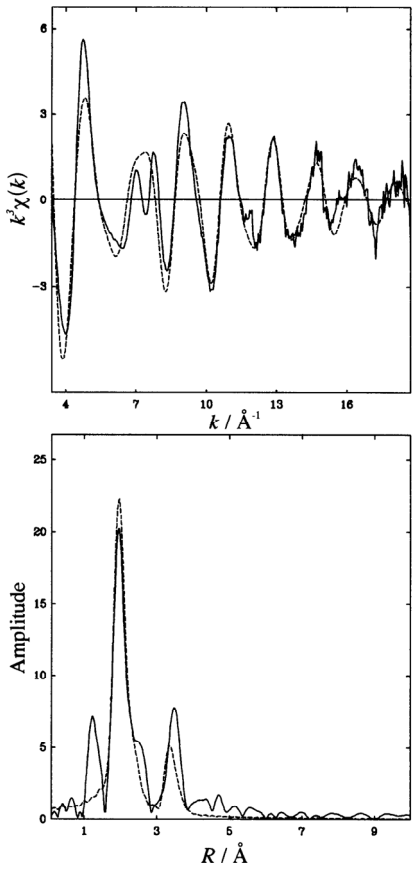

Fig. 5 Zr K-edge EXAFS for data unheated $(ZrO_2)_{0.1}(SiO_2)_{0.9}$ xerogel: k^3 weighted EXAFS (top) and Fourier transform (bottom). (———) Experimental data, and (– – – –) theoretical fit. Note that the experimental k^3 weighted EXAFS exhibits a double-electron transition at ~7.7 Å^{-1}.[20]

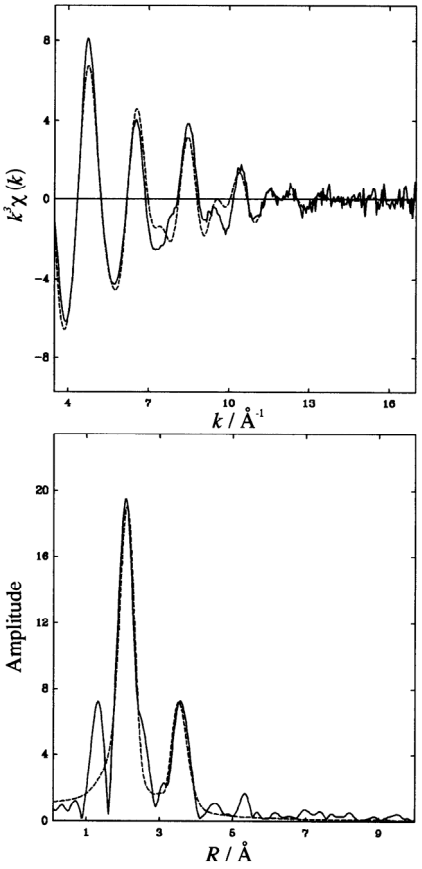

Fig. 6 Zr K-edge EXAFS for data unheated $(ZrO_2)_{0.4}(SiO_2)_{0.6}$ xerogel: k^3 weighted EXAFS (top) and Fourier transform (bottom). (———) Experimental data, and (– – – –) theoretical fit.

the calculated fits for the two extremes of composition, $(ZrO_2)_{0.1}(SiO_2)_{0.9}$ and $(ZrO_2)_{0.4}(SiO_2)_{0.6}$ after no heat treatment. These data illustrate a clear structural change over the composition range. The data from the $(ZrO_2)_{0.1}(SiO_2)_{0.9}$ samples are affected by a double-electron transition at ~7.7 Å^{-1},[20] as can be seen in Fig. 5. Consequently, during the fitting procedure for these samples, data were excluded between 7.0 and 8.3 Å^{-1}. It should be noted that the features at 1.5 Å in r-space are a characteristic of most oxides[21] and are artefacts of multiple scattering events. The shoulder at about 2.6 Å in r-space is more problematic. Okasaka *et al.*[22] ascribed the peak to non-bridging Zr–O bonds. However, this distance is too long for Zr–O bonding and it seems likely that the feature is an artefact of the Fourier transform.[23]

Discussion

The ^{29}Si MAS NMR results presented above show the general trend in all four samples of an increase in more polymerised Q^n species as the temperature of the heat treatment increases. It is well known that for SiO_2 sol–gels, heat treatment to progressively higher temperatures leads to the loss of organic groups and to further condensation which strengthens the silica network and eventually leads to the presence of only Q^4 species (*i.e.* virtually all of the SiO_4 tetrahedra are connected to four other SiO_4 units). The interesting feature of these NMR results concerns the effect that zirconium has on the chemical shift of silicon. Table 1 clearly shows that as the zirconium dopant level is increased, the extent of condensation of the silica network is reduced. It has been previously shown that in the related materials, $(TiO_2)_x(SiO_2)_{1-x}$, where $x < 0.2$, titanium adopts tetrahedral coordination within the silica network and has little effect on the silicon chemical shift.[24] Thus, for a $(TiO_2)_{0.18}(SiO_2)_{0.82}$ sample heated to 750 °C, virtually all the silicon is present as Q^4 species. Zirconium is therefore playing a very different role in these mixed oxide sol–gel materials compared to that of titanium. Other workers have observed similar behaviour in $(ZrO_2)_x(SiO_2)_{1-x}$ sol–gels. Tartaj *et al.*[25] observed a single broad peak at −89.3 ppm in the ^{29}Si MAS NMR spectrum from an unheated $(ZrO_2)_{0.5}(SiO_2)_{0.5}$ sample prepared by the hydrolysis of an aerosol of Zr and Si alkoxides. This band was attributed to the presence of silicon in $Si(SiO)_2(ZrO)_2$ (Q^2_{2Zr}) and $Si(SiO)(ZrO)_3$ (Q^1_{3Zr}) environments. Andrianainarivelo *et al.*[11] studied $(ZrO_2)_x(SiO_2)_{1-x}$ materials prepared by a non-hydrolytic sol–gel route and found that increasing the zirconium content lead to an increasing number of Zr–O–Si bonds, which, in turn, lead to an increase in the Q^2_{2Zr} and Q^3_{1Zr} signals in the ^{29}Si NMR spectra. The effect described above is due to the high field strength[13] of Zr^{4+} ions which cause them to adopt higher coordination numbers with respect to oxygen. Zr^{4+} cannot substitute tetrahedrally into a silica network as can Ti^{4+} and therefore acts as a network modifier. This disrupting effect is illustrated by the widths of the ^{29}Si NMR peaks which show a general increase with increasing Zr content. In fact, this network modifying behaviour has been cited as the cause of the catalytic activity of $(ZrO_2)_x(SiO_2)_{1-x}$ materials.[26]

The FTIR results shown in Figs. 1(a) and (b) illustrate the effect that zirconium has on the silica network. The main change observed in the spectra at both temperatures is that the silica network vibrations at 1160, 1070 and 795 cm^{-1} become less well defined as the zirconium content is increased. This effect is most pronounced for the 795 cm^{-1} peak due to the symmetric stretch of the SiO_4 unit[11,13] which has all but disappeared for the $(ZrO_2)_{0.4}(SiO_2)_{0.6}$ sample. Clearly, the addition of zirconium is modifying the connectivity and strength of the silica network.

The amount of zirconium present also causes a significant change in the size of the peaks at ~3550, ~3200 and 1640

cm^{-1} due to hydroxy groups and adsorbed water for the samples heat treated to 750 °C. Increasing the amount of zirconium increases of number of hydroxy groups present. This change can be rationalised in terms of the extra disorder introduced into the structure by the presence more ZrO_x ($x > 4$) polyhedra. The extra disorder is associated with the presence of more non-bridging M–O bonds. The fact that more adsorbed water is present at the higher levels of zirconium doping is most likely due to the presence of more hydroxy groups which provide sites for water to hydrogen bond.

The shoulder at $\sim$980 cm^{-1} changes shape and position with heat treatment and zirconium content. This feature has contributions from Si–(OH) stretches and Zr–O–Si modes, and for the unheated samples becomes stronger and less well defined as the zirconium content increases. Since the broad hydroxy band centred at $\sim$3400 cm^{-1} has similar intensity for all the unheated samples, it can be deduced that the change in the 980 cm^{-1} feature is due to an increase in the number of Zr–O–Si bonds with increasing zirconium content. The same conclusions cannot be drawn from the spectra from the heat treated samples since the concentration of hydroxy groups also increases with zirconium content.

The peaks at the low energy end of the spectra are more difficult to interpret. All spectra exhibit a broad feature at about 500 cm^{-1} with a weak shoulder at $\sim$600 cm^{-1}. Nogami[13] attributed intensity in the 500–600 cm^{-1} region of the IR spectra of $(ZrO_2)_x(SiO_2)_{1-x}$ sol–gels to the presence of ZrO_x polyhedra in which the Zr^{4+} ion does not enter the total anionic framework structure of the glass. Lee and Condrate[12] made a similar assignment, attributing a broad band at 600 cm^{-1} to the vibration of ZrO_x units in an atomic arrangement similar to that in crystalline cubic zirconia. It should be noted the pure sol–gel derived silica also exhibits IR absorption in the 400–600 cm^{-1} region; Matos *et al.*[27] observed bands at $\sim$550 and $\sim$460 cm^{-1} which were assigned to Si–(OH) and Si–O–Si bending vibrations, respectively. In the spectra presented here, there is a definite increase in intensity in the 500–600 cm^{-1} region with increasing zirconium content for both the unheated and heat treated samples. This suggests an increase in the number of interstitial ZrO_x units within the silica network as the zirconium content is increased.

The disappearance of the sharp bands at 2900 and 1450 cm^{-1} due to C–H vibrations with heat treatment provides evidence for the removal of any organic fragments with heating to 750 °C.

The Zr K-edge EXAFS parameters in Table 3 provide important information on the local environment of the zirconium atoms in these samples. The structural parameters derived for the $(ZrO_2)_{0.3}(SiO_2)_{0.7}$ and $(ZrO_2)_{0.4}(SiO_2)_{0.6}$ samples, before and after heat treatment, resemble those for monoclinic ZrO_2. The Zr–O nearest neighbour distances obtained are all close to the average value for monoclinic ZrO_2 obtained from this EXAFS study. The Zr–O coordination numbers are close to 8 but, taking into account the errors in coordination numbers derived from this technique ($\pm$20%), the difference between 7-fold and 8-fold coordination cannot be unambiguously distinguished. The distances obtained from the EXAFS technique, with uncertainties of $\pm$0.05 Å for nearest neighbour correlations, often provide a much better guide to local environment. The Zr–Zr distances in the $(ZrO_2)_{0.3}(SiO_2)_{0.7}$ and $(ZrO_2)_{0.4}(SiO_2)_{0.6}$ samples are between 3.4 and 3.5 Å which are close to the value of 3.46 Å found in monoclinic ZrO_2.

The Zr–Zr coordination numbers of just over 4 are much lower than the value of 7 expected for monoclinic ZrO_2. The Debye–Waller factors for the Zr–Zr shell in the xerogel samples are also significantly higher than those obtained from monoclinic ZrO_2, indicating much greater disorder in this shell for the former materials. Similar results have been obtained from EXAFS studies of amorphous $Zr(OH)_4$ prepared from zirconium basic sulfate.[28] Based upon the preceding observations, it is proposed that for the $(ZrO_2)_{0.3}(SiO_2)_{0.7}$ and $(ZrO_2)_{0.4}(SiO_2)_{0.6}$ samples before and after heat treatment a significant proportion of the ZrO_2 forms amorphous regions with Zr in a local environment close to that found in monoclinic ZrO_2.

The EXAFS data from the $(ZrO_2)_{0.1}(SiO_2)_{0.9}$ samples are best fitted with a different structural model consisting of a split Zr–O shell and one Zr–Zr distance. This distinct splitting of the Zr–O shell is similar to that observed in cubic and tetragonal zirconia,[5] and in zircon, $ZrSiO_4$.[9] The two Zr–O distances of $\sim$2.0 and $\sim$2.2 Å obtained are closest to those for yttrium stabilized cubic zirconia which has three oxygens at a distance of 2.04 Å and four oxygens at 2.23 Å. The Zr–Zr coordination numbers of $\sim$0.5 and distances of $\sim$3.4 Å are consistent with Zr being randomly distributed through the silica structure with no phase separation of ZrO_2. For example, a $(ZrO_2)_{0.1}(SiO_2)_{0.9}$ sample with a Zr–M coordination number of 8 (*cf.* zircon) and a random distribution of Zr would have a Zr–Zr coordination number of 0.8.

The structural parameters obtained for the $(ZrO_2)_{0.2}(SiO_2)_{0.8}$ samples are intermediate between those for the $(ZrO_2)_{0.1}(SiO_2)_{0.9}$ and $(ZrO_2)_{0.4}(SiO_2)_{0.6}$ samples. The high Debye–Waller factors of $\sim$0.04 $Å^2$ for the Zr–O shell suggests a possible splitting of this shell as observed in the $(ZrO_2)_{0.1}(SiO_2)_{0.9}$ samples whereas the Zr–Zr coordination numbers of close to 4 suggest a degree of phase separation of amorphous ZrO_2 as in the samples of higher Zr content. It seems likely that as the Zr content increases above 10 mol% phase separation of some amorphous ZrO_2 starts to occur; at 40 mol% Zr, a significant proportion of zirconium is present as amorphous ZrO_2. Similar results were obtained by Lee and Condrate[12] who identified ZrO_2-rich regions in $(ZrO_2)_x(SiO_2)_{1-x}$ sol–gel derived glasses for $x \geqslant 0.27$ from the presence of a broad band at 550 cm^{-1} in the Raman spectra. The results from the $(ZrO_2)_{0.1}(SiO_2)_{0.9}$ samples clearly show that when zirconium enters the silica network homogeneously, it acts as a network modifier, thus agreeing with the ^{29}Si NMR and FTIR results discussed above. Considering all the results presented in Table 3, it appears that heat treatment has little effect on the coodination of zirconium in these materials. One noticeable effect, is a general increase in the Debye–Waller factors for the Zr–O shells of the higher zirconium content samples. This may reflect more zirconium entering the silica network and a change in local coordination from monoclinic-like to cubic/tetragonal-like as the samples are heated.

The ^{17}O MAS NMR results shown in Figs. 3 and 4 complement the EXAFS results. The spectra from the $(ZrO_2)_{0.4}(SiO_2)_{0.6}$ samples all show the presence of Si–O–Si (0 ppm), Zr–O–Si (150 ppm) and Zr–O–Zr (295 and 395 ppm) bridges. As mentioned previously, the positions of the peaks due to Zr–O–Zr bonding are close to those observed from monoclinic zirconia.[18] This result suggests, in agreement with the interpretation of the EXAFS data, that these samples contain phase separated ZrO_2 with a local structure similar to that in monoclinic zirconia. The effect of heat treatment is to bring the peaks due to Zr–O–Zr bonding closer together and to broaden the Zr–O–Si peak. However, this probably reflects a change in local coodination of some of the zirconium atoms to an environment closer to that found in cubic and tetragonal zirconia; tetragonal zirconia exhibits a Zr–O–Zr peak at 365 ppm[18] which is approximately midway between the peaks from monoclinic zirconia. The spectra from the $(ZrO_2)_{0.1}(SiO_2)_{0.9}$ samples all show the presence of Si–O–Si (0 ppm) and Zr–O–Si (150 ppm) bridges and an absence of Zr–O–Zr bonding. These results support the interpretation of the EXAFS data showing that the $(ZrO_2)_{0.1}(SiO_2)_{0.9}$ samples

are atomically mixed. The Zr–O–Si peak becomes slightly more intense with heat treatment. This may reflect densification of the structure as hydroxy groups are lost and more Zr–O–Si bonds are formed. It should be noted that, despite phase separation, the spectra from the $(ZrO_2)_{0.4}(SiO_2)_{0.6}$ samples show more intense peaks due to Zr–O–Si bonding than those from the $(ZrO_2)_{0.1}(SiO_2)_{0.9}$ samples. This indicates that, although phase separation starts to occur at ~20 mol% Zr, the amount of isolated interstitial ZrO_2 within the silica network still increases as the zirconium content is raised.

Conclusions

All the structural techniques described above show that zirconium clearly behaves differently from titanium in mixed metal-oxide : silica materials prepared by the sol–gel method. Titanium can substitute for silicon in the silica network for low levels of doping whereas zirconium always acts as a network modifier. The network modifying behaviour of zirconium has been used Millar and Ko[26] to explain the high catalytic activity of $(ZrO_2)_x(SiO_2)_{1-x}$ aerogels compared with their titanium doped counterparts. The authors attribute the catalytic activity to acid sites which result from the "charge imbalance" in the Zr–O–Si bridges caused by mismatches in cation valency and coordination. EXAFS and ^{17}O MAS NMR data have shown that for $(ZrO_2)_{0.1}(SiO_2)_{0.9}$ samples the oxides are atomically mixed with no evidence of phase separation. In these samples the local structure of zirconium is similar to that found in cubic zirconia. The results for the $(ZrO_2)_{0.4}(SiO_2)_{0.6}$ samples show that some phase separation occurs with a significant proportion of the zirconium present as amorphous ZrO_2 with a local structure similar to that of monoclinic zirconia. The remaining ZrO_2 enters the interstices of the silica network. Despite phase separation, the $(ZrO_2)_{0.4}(SiO_2)_{0.6}$ samples contain more Zr–O–Si bonding than the $(ZrO_2)_{0.1}(SiO_2)_{0.9}$ samples. This observation highlights another difference between the role of zirconium and titanium in such materials. In $(TiO_2)_x(SiO_2)_{1-x}$ materials, when phase separation occurs at $x \sim 0.4$, nearly all the TiO_2 is present as a separate phase,[8] whereas in $(ZrO_2)_x(SiO_2)_{1-x}$ ($x > 0.2$) samples, phase separated ZrO_2 and interstitial ZrO_2 are present in equillibrium. Since the level of phase separation is crucial to the physical properties and usefulness of these materials, ^{17}O MAS NMR and EXAFS have proven valuable techniques for detecting this.

Acknowledgements

The EPSRC is thanked for its support of the characterisation of sol–gel produced materials through grant GR/L28647 and for the funding of Dr G. Mountjoy through grant GR/K95987.

References

1 R. G. Simhan, *J. Non-Cryst. Solids*, 1983, **54**, 335.
2 J. B. Millar, S. E. Rankin and E. I. Ko, *J. Catal.*, 1994, **148**, 673.
3 C. J. Brinker and G. W. Scherer, *Sol–Gel Science, The Physics and Chemistry of Sol–Gel Processing*, Academic Press, San Diego, 1990.
4 F. Farges, G. E. Brown Jr. and D. Velde, *Am. Miner.*, 1994, **79**, 838.
5 P. Li, I-W. Chen and J. E. Penner-Hahn, *Phys. Rev. B*, 1993, **48**, 10063.
6 R. J. Davis and Z. Liu, *Chem. Mater.*, 1997, **9**, 2311.
7 J. S. Rigden, R. J. Newport, M. E. Smith, P. J. Dirken and G. Bushnell-Wye, *J. Mater. Chem.*, 1996, **6**, 337.
8 P. J. Dirken, M. E. Smith and H. J. Whitfield, *J. Phys. Chem.*, 1995, **99**, 395.
9 R. M. Hazen and L. W. Finger, *Am. Miner.*, 1979, **64**, 196.
10 B. E. Yoldas, *J. Non-Cryst. Solids*, 1980, **38**, 81.
11 M. Andrianainarivelo, R. Corriu, D. Leclercq, P. H. Mutin and A. Vioux, *J. Mater. Chem.*, 1996, **6**(10), 1665.
12 S. W. Lee and R. A. Condrate Sr, *J. Mater. Sci.*, 1988, **23**, 2951.
13 M. Nogami, *J. Non-Cryst. Solids*, 1985, **69**, 415.
14 G. Engelhardt and D. Michel, *High Resolution Solid State NMR of Silicates and Zeolites*, Wiley, Chichester, 1987.
15 M. E. Smith, *Appl. Magn. Reson.*, 1993, **4**, 1.
16 M. E. Smith and H. J. Whitfield, *J. Chem. Soc., Chem. Commun*,. 1994, 723.
17 T. M. Walter, G. L. Turner and E. Oldfield, *J. Magn. Reson.*, 1988, **76**, 106.
18 P. J. Dirken, R. Dupree and M. E. Smith, *J. Mater. Chem.*, 1995, **5**, 1261.
19 N. Binstead, J. W. Campbell, S. J. Gurman and P. C. Stephenson, *EXAFS Analysis Programs*, Daresbury Laboratory, Warrington, 1991.
20 A. Filipponi and A. Di Cicco, *Phys. Rev. A*, 1995, **52**, 1072.
21 G. Antonioli, P. P. Lottici, I. Manzini, G. Gnappi, A. Montenero, F. Paloschi and P. Parent, *J. Non-Cryst. Solids*, 1994, **77**, 179.
22 K. Okasaka, H. Nasu and K. Kamiya, *J. Non-Cryst. Solids*, 1991, **136**, 103.
23 S. Pei, G. W. Zajac, J. A. Kadak and J. Faber, *Catal. Lett.*, 1993, **21**, 333.
24 D. M. Pickup, G. Mountjoy, G. W. Wallidge, R. Anderson, J. M. Cole, R. J. Newport and M. E. Smith, *J. Mater. Chem.*, 1999, **9**, in the press.
25 P. Tartaj, J. Sanz, J. Serna and M. Ocaña, *J. Mater. Sci*,. 1994, **29**, 6533.
26 J. B. Millar and E. I. Ko, *J. Catal.*, 1996, **159**, 58.
27 M. C. Matos, L. M. Ilharco and R. M. Almeida, *J. Non-Cryst. Solids*, 1992, **147 & 148**, 232.
28 X. Turrillas, P. Barnes, A. J. Dent, S. L. Jones and C. J. Norman, *J. Mater. Chem.*, 1993, **3**, 583.

Paper 9/01401B